Effect of Gadolinium and Thulium Doping on Phase Development, Structural, Micro-structural and Dielectric properties of SrTiO3-δ

Ramanjeet Kaur*, [1] and Anand K Tyagi[2]

[1]*Department of Applied Sciences, SBSSTC, I. K. Gujral Punjab Technical University, Kapurthala, 144603 (Punjab) India.*

[2]*Department of Applied Sciences, SBS State Technical Campus, NH-05, Firozpur 152004 (Punjab) India.*

Abstract: *In this work, gadolinium and thulium doped strontium titanate samples having composition $Sr_{1-x}Gd_xTi_{1-y}Tm_yO_{3-\delta}$ ($0 \leq x \leq 0.30$, $0 \leq y \leq 0.05$) have been successfully synthesized using sol gel method. All the synthesized ceramics possess sharp and well-defined XRD peak patterns without any impurity phases. The decrease in lattice parameter with increase in amount of Gadolinium was observed. X ray diffraction (XRD), scanning electron microscopy (SEM) and energy dispersive X ray analysis (EDX) studies confirm the formation of cubic $Sr_{1-x}Gd_xTi_{1-y}Tm_yO_{3-\delta}$ ($0 \leq x \leq 0.30$, $0 \leq y \leq 0.05$) perovskites. SEM/EDX analysis revealed that ceramics possess high density with marginal inter-granular porosity. The synthesized samples possess high dielectric constants, high ac conductivity and low loss factors which further enhanced with gadolinium and thulium doping.*

Key words*: Phase- development, Structural, Micro-structural, Dielectric properties, sol gel*

1. Introduction

Fuel cell is one of the leading options available as efficient and environment friendly technologies that can generate power from renewable fuels like hydrogen etc. A fuel cell can generate electricity from electrochemical reaction, with pure water and potentially useful heat as the byproducts. It can produce electricity as long as it is supplied the source of H_2 and O_2. Fuel cells offer many advantages over conventional energy sources like very low emissions; especially Green House Gases (GHGs), high efficiencies, lesser costs, flexibility in size etc. Various types of fuel cells are used nowadays including solid polymer proton conductor fuel cells (SPFCs), alkaline fuel cells (AFCs), phosphoric acid fuel cells (PAFCs), molten carbonate fuel cells (MCFCs) and solid oxide fuel cells (SOFCs). SOFCs are generally preferred over other fuel cells as they suffer from many fatal disadvantages like easily poisoning by carbon dioxide (CO_2) in AFCs, lesser durability of MCFCs, less efficiency and requirement of expensive catalyst leading to higher costs in PAFCs etc. SOFCs, however, overcome these problems having high efficiency, lesser cost, no need of catalyst owing to high operating temperatures etc [1-5].

Solid oxide fuel cells (SOFCs), thus, have recently emerged as a superior high temperature fuel cell technology owing to many advantages over conventional power-generating systems in terms of efficiency, reliability, modularity, fuel flexibility, and environmental friendliness [6-7]. The main components of SOFCs are anode, cathode and electrolyte. The

conventional materials i.e. nickel/copper – yttria stablized zirconia, rare earth doped ceria etc., used for the fabrication of different components of SOFCs, suffer from the various problems like sulfur poisoning, poor mechanical integrity, carbon deposition and lesser stability in reducing conditions. These problems put a major hurdle in commercializing this futuristic technology. The oxides with perovskite structure have emerged as good alternates as these can withstand the aforesaid problems. The most widely studied perovskites are Strontium titanates, Lanthanum chromites and their doped forms [8-12]. The doping of $SrTiO_{3-\delta}$ with various elements i.e. La, Ce, Sm, Gd, Dy, Y, Cu for Sr site and Fe, V, W, Mo, Ta, Nb for Ti site have been investigated by various research groups and enhancement in the ionic conductivity has been reported [13-14]. A number of synthesis routes have been employed to synthesize these perovskite materials in literature but all of them suffer from one or the other problems whereas sol gel based method offers a clean, contamination free and easy method for synthesizing these materials.

In the present work, we have reported the synthesis of Gd, Tm codoped $SrTiO_{3-\delta}$ ($Sr_{1-x}Gd_xTi_{1-y}Tm_yO_{3-\delta}$) samples for various compositions. Sol gel technique has been used to synthesize these materials. The structural characterization, micro-structural & morphological investigation, elemental compositional analysis and dielectric properties determination of all the synthesized materials have been thoroughly carried out using advanced characterization techniques.

2. Experimental Work

2.1. Synthesis

$Sr_{1-x}Gd_xTi_{1-y}Tm_yO_{3-\delta}$ samples for various values of x and y (x = 0, y = 0; x = 0.05, y = 0.005; x = 0.1, y = 0.005; x = 0.15, y = 0.02; x = 0.20, y = 0.02; x = 0.25, y = 0.05 and x = 0.30, y = 0.05) were synthesized using titanium tetra isopropoxide, strontium acetate, gadolinium Nitrate, thulium nitrate penta hydrate, propanol, hydrochloric acid (HCl) and distilled water as starting chemicals employing sol gel method as described in our earlier paper [15]. The obtained powders were calcined at 600°C and then sintered at 1250°C for 2 hours at heating rate 3°C per minute. The obtained powders were pelletized; the pellets were then calcined at 600°C for one hour and then further, sintered at 1250°C for 2 hours at heating rate of 3°C per minute. All the seven samples were prepared using the aforesaid technique in a single go.

2.2. Characterization

X ray diffraction analysis of the sintered pellets was done with the help of XPERT-PRO X-RAY diffractometer 0000000011059259 using Cu K_α radiation. SEM/EDX analysis of the prepared pellets was carried out using using JEOL for morphological and elemental analysis. The dielectric properties of the sintered the samples were studied with the help of LCR Impedance Analyzer.

3. Results and Discussion

3.1. XRD Analysis

XRD peak patterns of $Sr_{1-x}Gd_xTi_{1-y}Tm_yO_{3-\delta}$ samples (0≤x≤0.30, 0≤y≤0.05) are shown in Figure 1. Clearly, all the XRD peaks are well defined and are indexed on the basis of cubic symmetry of the structure using mathematical method [16]. The XRD patterns observed here are similar to the XRD pattern of $SrTiO_3$ reported in literature [17]. All the STO samples show nearly identical XRD patterns with no detectable impurity phases indicating the purity of the synthesized ceramics. XRD peaks are more intense and sharper for

samples synthesized here after sintering than that for calcined samples as reported in our earlier paper [15] revealing the better phase development with sintering.
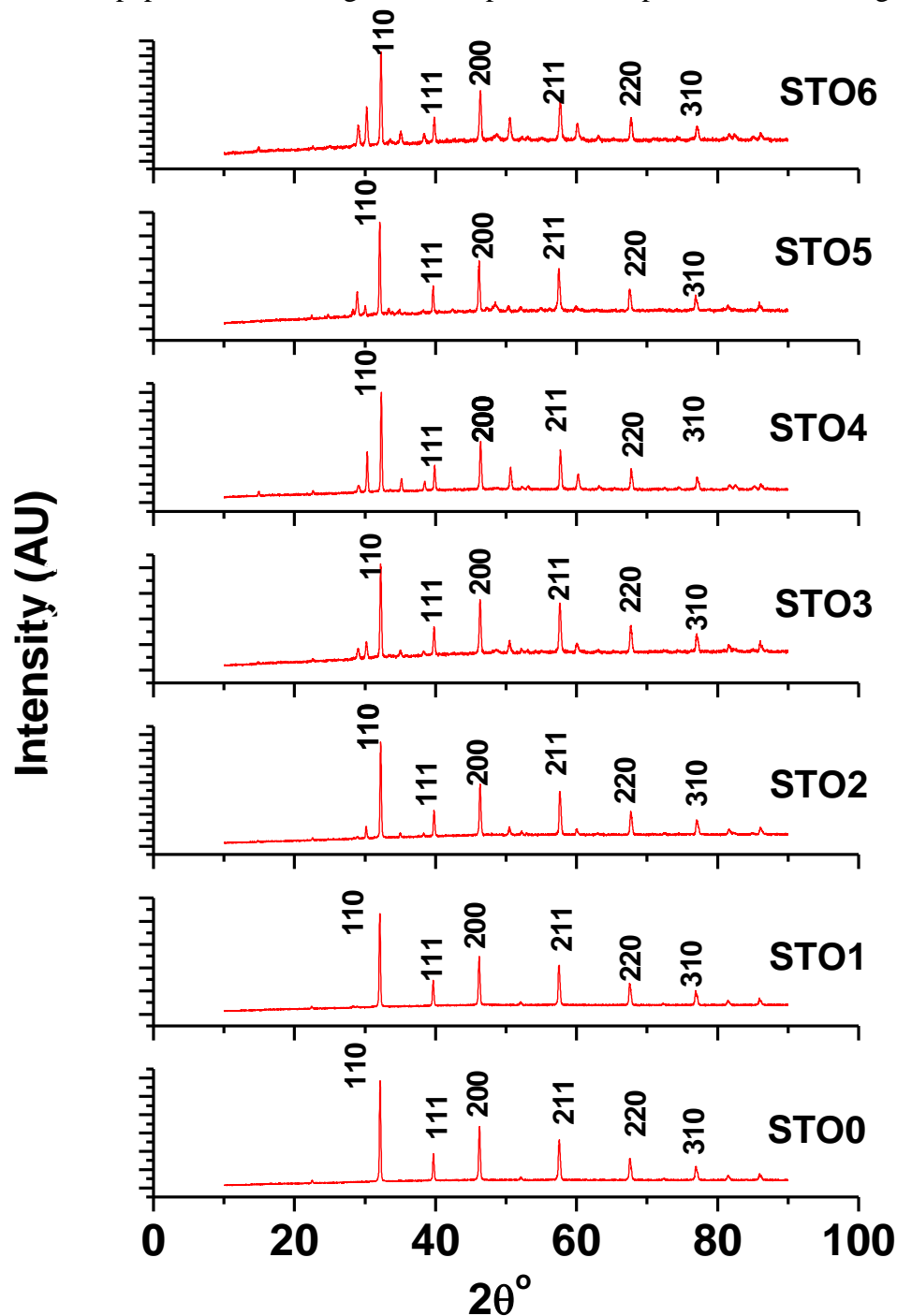
Figure 1. XRD Peak Pattern for $Sr_{1-x}Gd_xTi_{1-y}Tm_yO_{3-\delta}$ Samples (0≤x≤0.30, 0≤y≤0.05)

The shift of most intense peak (110) for $Sr_{1-x}Gd_xTi_{1-y}Tm_yO_{3-\delta}$; STO samples from pure sample i.e. STO0 with increase in gadolinium content and constant doping amount of thulium is shown in Figure 2. It can be observed from the figure that peaks for STO1 and STO3 samples shift slightly toward smaller angle with respect to the peak of STO0; pure undoped $SrTiO_{3-\delta}$ whereas the peak-shift toward larger angle can be observed in STO1 to STO2, STO3 to STO4 and STO5 to STO6 samples. The peak shift toward smaller angle can be attributed to intake of relatively larger ion Tm^{3+}; ionic radius 88 pm, as a replacement

of Ti^{4+} ions; ionic radius 60.5 pm.   Whereas the peaks shift toward the large angle as we move from STO1 to STO2, STO3 to STO4 and STO5 to STO6 samples can be due to increase in Gadolinium content at constant amount of thulium. The Gd^{3+} ions (ionic radius 107.8 pm) used as a replacement of Sr^{2+} ions (ionic radius 132 pm), being smaller in size, lead to this shift [13, 18].
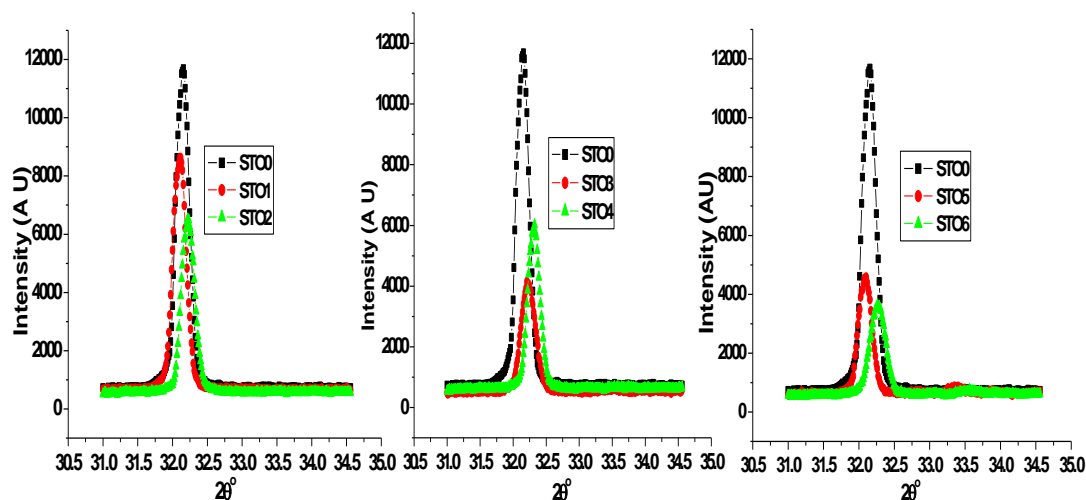
Figure 2. Shift of the Most Intense Peak (110) for $Sr_{1-x}Gd_xTi_{1-y}Tm_yO_{3-\delta}$ Samples (0≤x≤0.30, 0≤y≤0.05) with Increase in 'Gd' Content.

Table 1. Lattice Parameter Values for $Sr_{1-x}Gd_xTi_{1-y}Tm_yO_{3-\delta}$ Samples

Sample Code	x	y	Lattice Parameter (Å)
STO0	0	0	3.9249
STO1	0.05	0.005	3.9259
STO2	0.1	0.005	3.9169
STO3	0.15	0.02	3.9157
STO4	0.2	0.02	3.9105
STO5	0.25	0.05	3.9265
STO6	0.3	0.05	3.9196

The lattice parameter 'a' values for the synthesized $Sr_{1-x}Gd_xTi_{1-y}Tm_yO_{3-\delta}$ samples were calculated using mathematical method for cubic crystals [16] and are included in table 1. It can be clearly revealed that lattice parameter 'a' decreases from STO1 to STO2, STO3 to STO4 and STO5 to STO6. The decrease in the lattice parameter, here, is caused by replacement of Sr^{2+} (132pm) by the smaller rare-earth element Gd^{3+} (107.8pm) [18]. The slight increase of lattice parameter in STO1 and STO5 samples in comparison to STO0 sample; the pure undoped sample may be attributed to substitution of titanium ion (Ti^{4+}; ionic radius ~ 60.5) by relatively larger thulium ion (Tm^{3+}; ionic radius ~88pm) along with substitution of strontium ion (Sr^{2+}; ionic radius ~ 132pm) by relatively smaller gadolinium ion (Gd^{3+}; ionic radius ~107pm).

The crystallite sizes for all the synthesized samples were calculated for (110) reflection; the peak with maximum intensity, using the Sherrer's equation [19]. All the $Sr_{1-x}Gd_xTi_{1-}$

$_yTm_yO_{3-\delta}$ samples, synthesized here after sintering, have crystallite size lying in the range from 28 to 35 nm, smaller than that reported in our earlier paper for STO samples obtained without sintering [15]. The decreased crystallite size, sharper & more intense XRD peaks,

for sintered samples revealed the increased crystalline nature of sintered samples having better phase development.

3.2. SEM Analysis
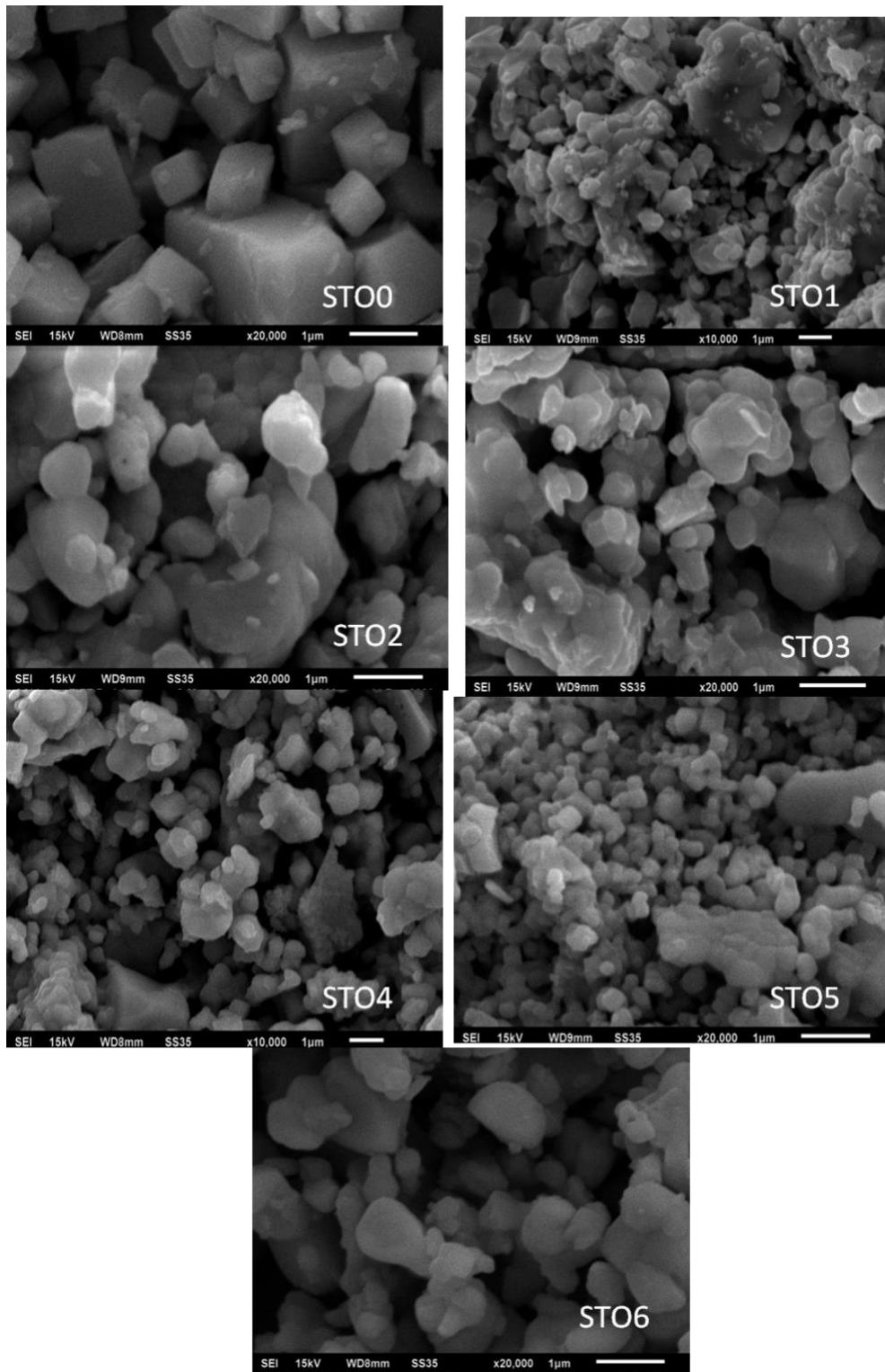
Figure 3. SEM Images of $Sr_{1-x}Gd_xTi_{1-y}Tm_yO_{3-\delta}$ Samples ($0\leq x\leq0.30$, $0\leq y\leq0.05$)

SEM micrographs of all $Sr_{1-x}Gd_xTi_{1-y}Tm_yO_{3-\delta}$; STO ($0\leq x\leq0.30$, $0\leq y\leq0.05$) samples obtained after sintering at 1250°C are shown in Figure 3. Clearly, all the samples are dense

having homogeneous microstructure with well developed small angular grains. The grain shape is cubiodal for STO0 (x=0, y=0) sample whereas the grains have isotropic shapes close to spherical one for STO1 (x=0.05, y=0.005) to STO6 (x=0.30, y=0.05) samples. The grain boundaries for all the prepared samples are smooth and clear having straight edges, well defined corners, faces without any extra phase precipitation. The straight edges confirm the high crystalline nature of the obtained ceramics, similar also revealed by XRD analysis. The synthesized STO samples have good sinterabiltiy and the low amount of inter-granular porosity as indicated by few residual and isolated voids present in the micrographs of STO samples. The microstructures of $Sr_{1-x}Gd_xTi_{1-y}Tm_yO_{3-\delta}$; STO samples have almost identical features, differing only in grain sizes. The average grain sizes for doped $SrTiO_{3-\delta}$ (STO) samples as obtained from SEM analysis are 728 nm, 583 nm, 576 nm, 514 nm, 424 nm, 369 nm and 325 nm for STO0, STO1, STO2, STO3, STO4, STO5 and STO6 respectively; clearly in the nano range. The grain sizes of the samples synthesized here after sintering are smaller than that for the samples without sintering as reported in our earlier paper; indicating that sintering leads to better grain growth. Also, it can be easily realized that increase in Gadolinium and Thulium doping leads to gradual decrease of grain size; with minimum value of grain size for STO6 [13, 20]. Thus, the high purity rare earth doped $SrTiO_{3-\delta}$ materials with high density have been successfully obtained by sol gel process at relatively lower sintering temperature.

3.3. EDX Analysis
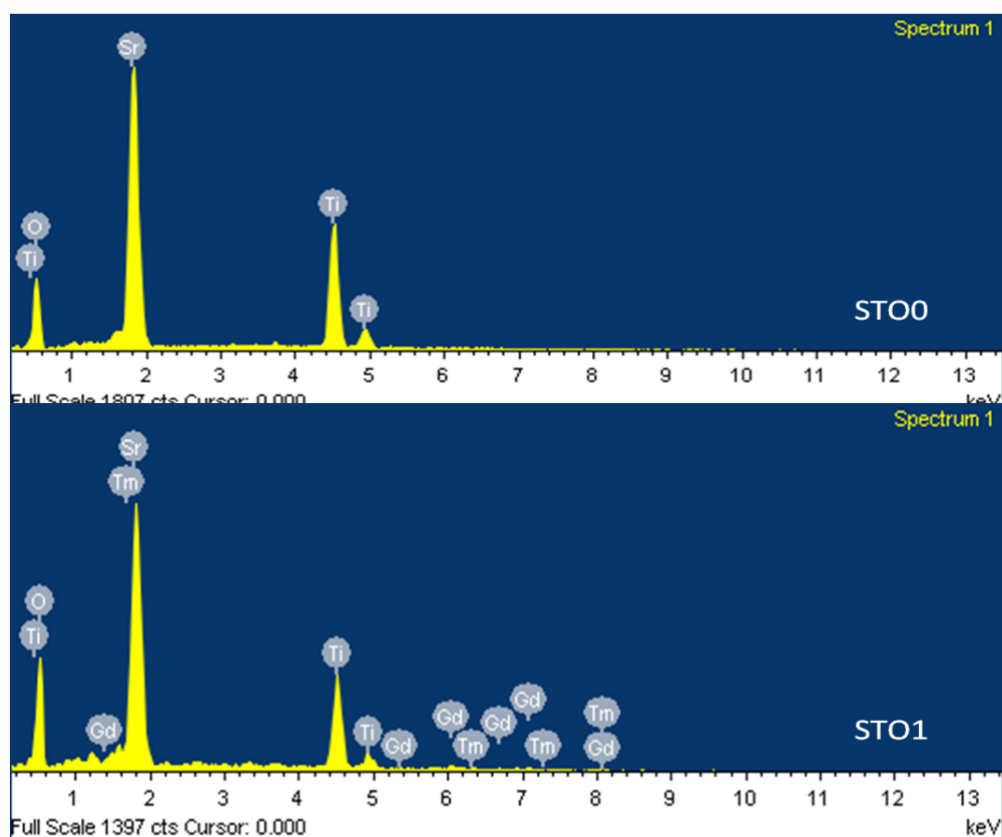
Figure 4. EDX Spectra for Samples STO0 (x=0, y=0) and STO1(x = 0.05, y = 0.005)

Figure 4 includes the EDX spectra for samples STO0 (x=0, y=0) and STO1(x = 0.05, y = 0.005) which reveal that only strontium, titanium and oxygen are present in STO0 however, along with these elements, gadolinium and thulium are also present in STO1 sample. EDX spectra for samples from STO2 to STO6 were also similar to STO1; having only strontium,

titanium, gadolinium; thulium and oxygen elements. There was no evidence for any other element confirming the purity of the synthesized STO samples. Table 2 includes the atomic ratios of the elements for all the $Sr_{1-x}Gd_xTi_{1-y}Tm_yO_{3-\delta}$ samples ($0 \leq x \leq 0.30$, $0 \leq y \leq 0.05$) as obtained from EDX analysis, which are almost same as elemental ratio i.e. Sr + Gd : Ti + Tm : O = 1 : 1 : 3, calculated theoretically.

Table 2. Atomic Ratio of Elements for $Sr_{1-x}Gd_xTi_{1-y}Tm_yO_{3-\delta}$ Samples ($0 \leq x \leq 0.30$, $0 \leq y \leq 0.05$) from EDX Analysis

Sample Code	x	y	Sr + Gd	Ti + Tm	O
STO0	0	0	1.04	1	4.53
STO1	0.05	0.005	1.12	1	5.00
STO2	0.10	0.005	1.15	1	4.89
STO3	0.15	0.02	0.96	1	6.04
STO4	0.20	0.02	1.33	1	5.34
STO5	0.25	0.05	0.94	1	6.39
STO6	0.30	0.05	1.01	1	5.29

The weight composition of all the synthesized $Sr_{1-x}Gd_xTi_{1-y}Tm_yO_{3-\delta}$; STO samples as obtained from EDX analysis is given in the table 3. It is evident from the data included in the table that amount of gadolinium increases from STO0 to STO6 as expected and that of thulium also increases as desired.

Table 3. Weight Composition of $Sr_{1-x}Gd_xTi_{1-y}Tm_yO_{3-\delta}$ Samples ($0 \leq x \leq 0.30$, $0 \leq y \leq 0.05$) from EDX Analysis

STO	Sr	Ti	Gd	Tm	O
STO0	1	0.50	0	0	0.81
STO1	1	0.52	0.096	0.052	0.96
STO2	1	0.56	0.17	0.069	0.99
STO3	1	0.46	0.37	0.23	1.40
STO4	1	0.59	0.36	0.23	1.49
STO5	1	0.49	0.48	0.13	1.09
STO6	1	0.66	0.69	0.24	1.42

3.4. Dielectric Characterization

The dielectric properties i.e. real and imaginary parts of dielectric constant, loss tangent, A C conductivity, Impedance etc. were analyzed using the LCR meter in the frequency range 100Hz to 1 MHz between 30 - 400°C temperatures. The real part of dielectric c onstant (ϵ_r) showed decrease with frequency as shown in figure 5 (a) which may be due to the reason that at low frequency, contribution from electronic, ionic, orientation and space charge polarization exist but at high frequency only electronic polarization or some contribution from ionic polarization [21] i s t here. The di electric c onstant (ϵ_r) increased with increase in temperature (300–400°C). The space charge polarization arising from the movement of ions and defects in the material may be responsible for this increase [22]. There was no curie peak detected in the whole measurement temperature range [23-24]. The dielectric constant value for pure sample was measured to be ~ 64 at frequency 1 KHz and at temperature 400°C. The dielectric constant values were 212, 190, 255.8, 270.03, 241.5 and 173.3 (at frequency 100Hz and temperature 400°C); 151, 123, 141, 148, 178 and 108 (at frequency 1 KHz and temperature 400°C) for STO1, STO2, STO3, STO4, STO5 and STO6 samples respectively, clearly higher values than that for pure sample.
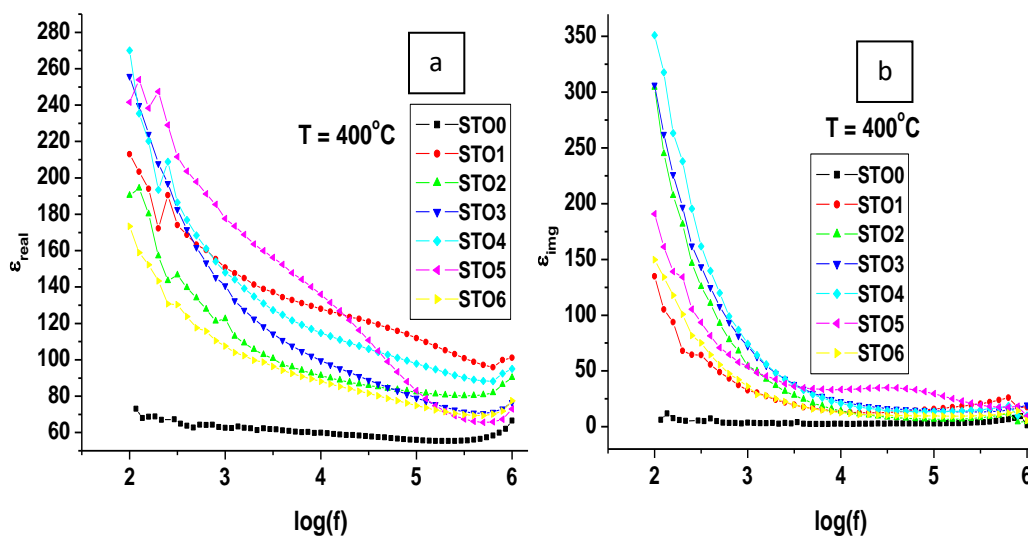
Figure 5. Variation of (a)Real Part of Dielectric Constant (b) Imaginary Part of Dielectric Constant with Frequency at 400^{0}C for Sr$_{1-x}$Gd$_x$Ti$_{1-y}$Tm$_y$O$_{3-\delta}$ (0≤x≤0.30, 0≤y≤0.05) Samples

Figure 5(b) shows the frequency dependence of imaginary dielectric constant (ε″) for doped SrTiO$_{3-\delta}$ samples at temperature 400ºC. The imaginary component of dielectric constant (ε″) showed the similar trends as that of ε$_r$ i.e. increase with temperature and decrease with frequency without any loss peak in the whole frequency spectrum of ε″. The values of ε″ are high only at low frequencies (below 1KHz) and at high temperature (300ºC to 400ºC) owing to the interfacial build up of the free charges either within the sample (Maxwell-Wagner (MW) polarization) [25] or between sample and the electrodes (space-charge polarization). The imaginary component of dielectric constant (ε″) for pure undoped SrTiO$_{3-\delta}$ sample is 0.340 at frequency 10 KHz and temperature 108ºC. It was found that doping led to increase in imaginary component of dielectric constant e.g. ε″ values were 3.241, 0.5161, 0.7348, 0.9396, 0.8438 and 0.415 for STO1, STO2, STO3, STO4, STO5 and STO6 respectively, at frequency 10 KHz and temperature 108ºC; clearly higher values than that for pure sample.
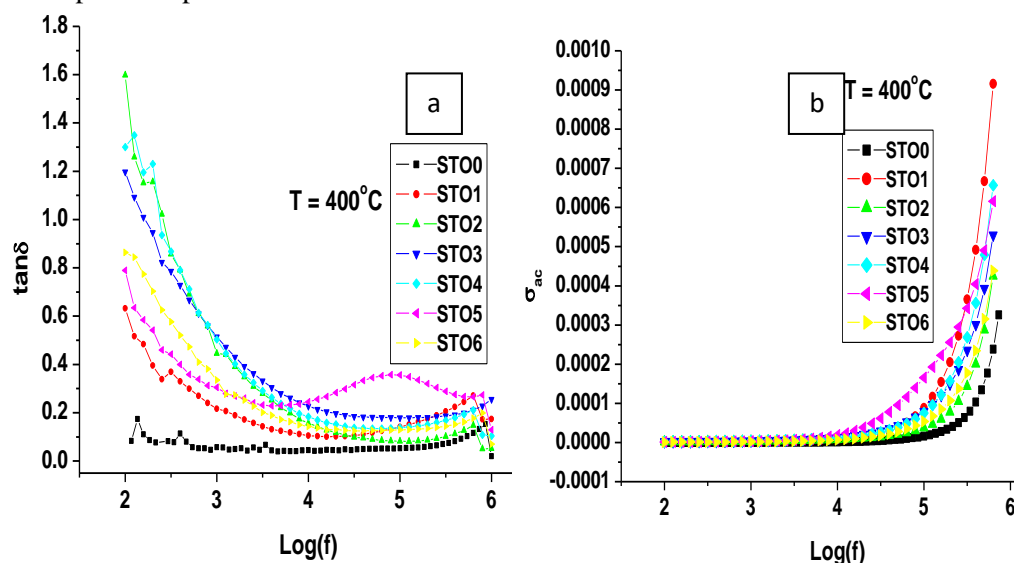
Figure 6. Variation of (a) Dielectric Loss (b) A C Conductivity with Frequency at 400ºC for Sr$_{1-x}$Gd$_x$Ti$_{1-y}$Tm$_y$O$_{3-\delta}$ (0≤x≤0.30, 0≤y≤0.05) Samples

The decrease in the loss tangent (tanδ) factor with frequency as shown in Figure 6(a) and increase with temperature was observed. The observed enhancement in loss factor values at high temperature can be due to transportation of thermally energetic ions. The dielectric loss for the $SrTiO_{3-\delta}$ measured at temperature below 250°C shows very small loss e. g. 0.00604 at frequency 10 KHz and temperature 108°C but by increasing the temperature from 250°C to 400°C, the dielectric loss value increased. The variation trends for the doped samples were approximately identical to that for undoped pure $SrTiO_{3-\delta}$ sample and increase in loss factor with doping was observed. The dielectric loss tangent values were 0.30, 0.0059, 0.0098, 0.011, 0.0116 and 0.0060 for STO1, STO2, STO3, STO4, STO5 and STO6 respectively at frequency 10 KHz and temperature 108°C.

AC conductivity was found to be almost constant at lower frequencies; while at higher temperatures and frequencies there was sharp enhancement in AC conductivity acquiring approximately 4.6 x 10^{-4} value at frequency 1 MHz and temperature 400°C; this increase may be due to the strong hopping mechanism [26]. Figure 6(b) shows the frequency dependence of AC conductivity at temperature 400°C. A plateau in the curves at low frequency and dispersion at high frequencies can be observed in the spectra. The transportation of the mobile ions due to applied field may be responsible for the observed plateau [27]. The observed trends of AC conductivity for doped samples were similar to pure $SrTiO_{3-\delta}$ sample and enhancement in it was observed with thulium and gadolinium doping e.g. AC conductivity values were 9.8 x 10^{-4}, 4.25 x 10^{-4}, 1.094 x 10^{-3}, 5.52 x 10^{-4}, 8.14 x 10^{-4} and 6.34 x 10^{-4} for x = 0.05, y = 0.005; x = 0.1, y = 0.005; x = 0.15, y = 0.02; x = 0.20, y = 0.02; x = 0.25, y = 0.05 and x = 0.30, y = 0.05 respectively at frequency 1 MHz and temperature 400°C, all higher than that for pure sample.
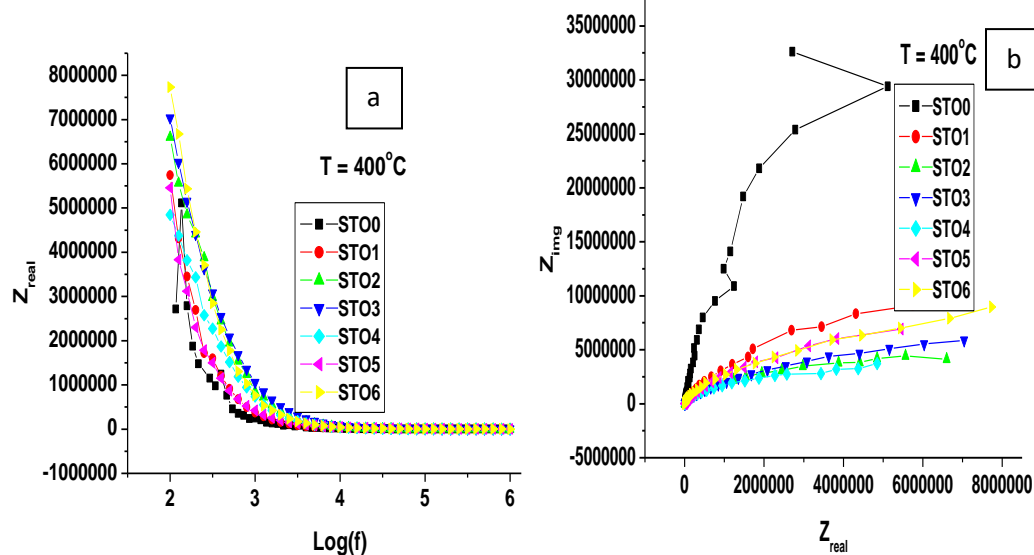
Figure 7. Variation of (a) Real Part of Impedance with Frequency (b) Cole-Cole Plots between Real Part (Z') and Imaginary Part (Z'') of Impedance at Temperature 400^{0}C for $Sr_{1-x}Gd_xTi_{1-y}Tm_yO_{3-\delta}$ (0≤x≤0.30, 0≤y≤0.05) samples

Figure 7(a) shows the variation of the real part of impedance (Z') for all doped STO samples with frequency at 400°C. The decrement in real component of impedance (Z') with frequency as well as with temperature was observed. The rise in temperature reduces the barrier which in turn leads to increase in ac conductivity and thus decrement in Z' e.g. the real impedance value for the pure sample reduced from 582883 (at room temperature) to 251586 (at 400°C) ; both determined at frequency 1KHz. The variation trends of real impedance (Z') with frequency and temperature for all the doped samples were similar to that of pure STO0 sample; Z' values were measured to be 69, 334.2, 104.8, 1060.9, 105.7, 321.8 and 110.14 for STO1, STO2, STO3, STO4, STO5 and STO6 samples respectively at

frequency 1 MHz and temperature 309°C. Figure 7(b) shows the Cole-Cole plots (Nyquist plots) of doped STO ceramic samples at 400°C. All the doped samples almost show the similar plots and radius of semicircle decreases with doping of gadolinium and thulium which shows that resistance decreases with doping [28].

Conclusion

In this work, $Sr_{1-x}Gd_xTi_{1-y}Tm_yO_{3-\delta}$ (0≤x≤0.30, 0≤y≤0.05) samples were successfully synthesized using low temperature sol gel technique and then, sintered at 1250°C. All the synthesized samples have sharp and well defined XRD patterns with crystallite size in nanometer range. The microstructures of the synthesized STO samples are homogeneous, less porous and crystalline having nano-metric grains. The doping with Gd and Tm further reduces the grain size. EDX analysis suggested that the ratio of strontium, titanium, thulium, gadolinium and oxygen is in close agreement with theoretical values. Thus, XRD and SEM/EDX studies reveal the formation of phase pure $Sr_{1-x}Gd_xTi_{1-y}Tm_yO_{3-\delta}$ samples having cubic structure. All the synthesized STO samples possess high dielectric constants, high ac conductivity and low loss factors which show further enhancement with doping.

Acknowledgements

REFERENCES

[1] T. Huria, Fuel cell basics, pp.1-5.

[2] Fuel Cell Handbook, Seventh Edition, EG&G Technical Services, Morgantown, West Virginia 26507-0880, 7-12, November 2004.

[3] S. D. Vora, in "Proceedings of the Fourth European Solid Oxide Fuel Cell Forum", Editor: McEvoy A. J., Lucerne, Switzerland, vol. 2, (2000), pp. 175.

[4] J. Sukkel, in "Proceedings of the Fourth European Solid Oxide Fuel Cell Forum", Editor: McEvoy A. J., Lucerne, Switzerland, vo. 2, (2000), pp. 159.

[5] H. Yokoyama, A. Miyahara and S. E. Veyo, in "Proceedings of the Fifth International Symposium on Solid Oxide Fuel Cells (SOFC-V)", Editors: Stimming U., Singhal S. C., Tagawa H., Lehnert W., Aachen, Germany, vol. 94, (1997).

[6] N. Q. Minh, Journal of American Ceramic Society, vol. 76, (1993), pp. 563.

[7] S. C. Singhal, MRS Bulletin, vol. 25, (2000), pp. 16.

[8] R. Mukundan, E. L. Brosha and F. H. Garzon, Electrochemical and Solid-State Letters, vol. 7, (2004), pp. A5–A7.

[9] Z. Cheng, S. Zha and M. Liu, Journal of Electrochemical Society, vol. 153, (2006), pp. A1302– A1309.

[10] Morales J. C. R., Vázquez J. C., Savaniu C., Marrero López D., Zhou W. and Irvine J. T. S., Nature, Vol. 439, 2006, pp.568.

[11] P. Blennow, K. K. Hansen, L. R.Wallenberg and M. Mogensen, Solid State Ionics, vol.180, (2009), pp. 63–70.

[12] K. Radhakrishnan, C. L. Tan, H. Q. Zheng and G. I. Ng, Journal of Vaccum Science Technology, vol.1638, (2000), pp.A 18.

[13] L. Zhang, T. Tosho, N. Okinaka and T. Akiyama, Materials Transactions, vol. 48, no. 8, (2007), pp. 2088-2093.

[14] M. Tolczyk, S. Molin, M. Gazda and P. Jasinski, Ceramic Materials, vol. 63, no. 1, (2011), pp. 151-156.

[15] R. Kaur and A. K. Tyagi, Journal of University of Shanghai for Science and Technology, vol. 22, (2020), pp. 1466-1479.

[16] Laboratory Module, Indexing X-Ray Diffraction Patterns.

[17] A. Rocca, A. Licciulli, M. Politi and D. Diso, International Scholarly Research Network Ceramics, (2012).

[18] R. D. Shannon, Acta Crystallographica, vol. A 32, (1976), pp. 751–767.

[19] B. D. Cullity, "Elements of X-Ray Diffraction", Addison-Wesley, 2nd edition, (1978).

[20] M. V. Makarovaa, A. Artemenkoa, J. Kopecek, F. Laufek, P. Zemenovaa, V. A. Trepakov and A. Dejnekaa, Scripta Materialia,vol. 116, (2016), pp. 21–25.

[21] A. Verma, O. P. Thakur, C. Prakash, T. C. Goel and R. G. Mendiratta, Material Science and Engineering B, vol. 116, no. 1, (2005).

[22] P. Abhijit and B. Amitabha, Journal of Material Science: Materials in Electronics, vol. 24, (2013), pp. 1855–1862.

[23] N. F. Muhamad, R. A. M. Osman, M. S. Idris and M. N. M. Yasin, EPJ Web Conf., vol.162, (2017), pp.01052.

[24] W. Li, Z. Ma, L. Gao and F. Wang, Materials, vol. 8, (2015), pp. 1176-1186.

[25] S. Kumar and K. B. R. Varma, Solid State Communications, vol. 147, (2008), pp. 457–460.

[26] K. C. B. Naidu, T. S. Sarmash and T. Subbarao, International Journal of Engineering Research & Technology, vol. 3, no. 1, (2014).

[27] T. Badapanda, R. K. Harichandan, A. Mishra and S. Anwar, Processing and Application of Ceramics, vol. 8, no. 3, (2014), pp. 145–153.

[28] S. Sahoo, U. Dash, S. K. S. Parashar and S. M. All, Journal of Advanced Ceramics, vol. 2, no. 3, (2013), pp. 291–300.